Catalysis Today 175 (2011) 93–99

Contents lists available at ScienceDirect

Catalysis Today

journal homepage: www.elsevier.com/locate/cattod

Carbon oxidation with Ag/ceria prepared by self-dispersion of Ag powder into nano-particles

Ken-ichi Shimizu[a,1], Hiroshi Kawachi[a], Shin-ichi Komai[b], Kaname Yoshida[c], Yukichi Sasaki[c], Atsushi Satsuma[a,*]

[a] Graduate School of Engineering, Nagoya University, Furo-cho, Chikusa-ku, Nagoya 464-8603, Japan
[b] Graduate School of Environmental Studies, Nagoya University, Furo-cho, Chikusa-ku, Nagoya 464-8603, Japan
[c] Japan Fine Ceramics Center, 2-4-1 Mutsuno, Atsuta-ku, Nagoya 456-8587, Japan

ARTICLE INFO

Article history:
Received 13 October 2010
Received in revised form 5 March 2011
Accepted 17 March 2011
Available online 5 May 2011

Keywords:
Carbon oxidation
Silver
Ceria
Self-dispersion
DPF

ABSTRACT

This study reports a unique and novel method of preparation of Ag/CeO_2 catalyst for carbon oxidation. A calcination of physical mixture of Ag metal powder and CeO_2 at 500 °C results in self-dispersion of Ag into nano-particles on CeO_2. From TEM images, the average diameter of Ag particles in Ag power before calcination was around 66 nm, while the particle size of Ag became smaller around 8 nm with very narrow distribution. Oxygen vacancy on CeO_2 surface is suggested to play an important role in the self-dispersion of Ag. The obtained catalyst showed high activity for soot oxidation comparable to Ag/CeO_2 prepared by impregnation method. The promotion effect of CeO_2 was not observed in physical mixtures with Cu, Au and Pt. Mechanical mixtures of Ag and various metal oxide supports were also examined. The addition of Ag to CeO_2, SnO_2, ZrO_2, ZnO, TiO_2, and Nb_2O_5 significantly lowered the temperature of carbon oxidation than those of supports, while that to Co_3O_4, CaO, La_2O_3, NiO, SiO_2, Al_2O_3 and MgO did not.

1. Introduction

The emission control of nitrogen oxides (NO*x*) and particulate matter (PM, mainly composed of soot and soluble organic compounds) is strongly required for clean diesel engine cars. As for the removal of PM, DPF (diesel particle filters) is known to be an effective technology to trap soot in exhausts. In a conventional DPF, the trapped soot is removed by continuous or periodical oxidation by heating DPF around 600 °C using external heating or injection of excess fuels into exhausts. These strategies lead to a decrease of overall fuel efficiency or an uncontrolled exotherm, which can destroy a filter. Therefore, a catalyzed soot oxidation is desired to decrease the soot burn-off temperature [1]. Many types of materials for catalyzed DPF have been reported so far. The proposed catalysts can be roughly classified into transition-metal oxides and perovskites [2–12], supported alkalines [13–15], supported metals [16–20], and ceria- or lanthanides-based catalysts [21–44]. Teraoka and Kagawa reported that perovskite- and spinel-type oxides, such as $Cu_{0.95}K_{0.05}Fe_2O_4$, show higher activity for simultaneous catalytic NO*x*-soot removal than Pt supported catalysts and pure metal oxides [3]. Supported alkaline catalysts usually show very high activity in loose contact mode. Ogura et al. reported that potassium-doped sodalite shows high activity and also high stability in a repeated run [14].

Recently, ceria based catalysts have been paid much attention because of very high activity with low ignition temperature. Makkee and co-workers examined active oxygen species on ceria and its role in soot oxidation [26–28]. From an isotope study using TAP technique, they demonstrated that gas phase oxygen is exchanged with lattice oxygen creating highly active oxygen species. They proposed that the active species should be adsorbed peroxide or superoxide, which spillover onto the soot surface and oxidize soot at lower temperatures. Machida et al. showed that the addition of Ag significantly promoted the oxidation activity of CeO_2 [35]. By using ESR spectra and $^{18}O_2$ pulse reaction, they demonstrated the formation of superoxide as active oxygen species, and proposed two possible reaction pathways. One is oxidation by reactive superoxide adsorbed at three-phase boundary between soot, reduced CeO_2, and gas phase. Another is reaction between active lattice oxygen and soot at ceria/soot interface. Aneggi et al. clearly showed TEM images of Ag catalysts supported on CeO_2, ZrO_2, and Al_2O_3 [37]. In their case, Ag/CeO_2 showed lower oxidation activity relative to Ag/ZrO_2, which was correlated to too much stabilized interface of $Ag/Ag_2O/CeO_2$.

Usually, Ag/CeO_2 catalysts are prepared by an impregnation method using an aqueous media [35,37,44]. In the present study,

* Corresponding author. Tel.: +81 52 789 4608; fax: +81 52 789 3193.
E-mail address: satsuma@apchem.nagoya-u.ac.jp (A. Satsuma).
[1] Present address: Catalysis Research Center, Hokkaido University, Kita 21, Nishi 10, Kita-ku, Sapporo 001-0021, Japan.

0920-5861/$ – see front matter © 2011 Elsevier B.V. All rights reserved.
doi:10.1016/j.cattod.2011.03.053

we report a unique and novel preparation method of Ag/CeO_2 catalyst for carbon oxidation. A physical mixture of Ag metal powder and CeO_2 followed by calcination at 500 °C results in self-dispersion of Ag into nano-particles, and the obtained catalyst shows high activity for carbon oxidation at low temperatures comparable to Ag/CeO_2 prepared by impregnation method. The similar promotion effect was also observed when SnO_2, ZrO_2, ZnO, TiO_2, and Nb_2O_5 were used as supports. The controlling factor for the self-dispersion is also discussed.

2. Experimental

2.1. Catalyst preparation

CeO_2 (JRC-CEO-1, 157 $m^2\,g^{-1}$) was supplied from Catalysis Society of Japan. $Ag + CeO_2$ catalysts (Ag loading = 5–60 wt%) were prepared by a mechanical mixing of Ag power (purchased from Kishida Chemical) and CeO_2 in a mortar for 5 min, followed by calcination in air at 500 °C for 3 h. The catalyst name is designated as $Ag(x) + CeO_2$, where x is the Ag loading in wt%. Metal powders were purchased from Mitsuwa Chemistry (Pt, Pd, Au) or Kishida Chemical (Cu). Ag_2O was purchased from Mitsuwa Chemistry. Metal oxide supports of ZrO_2 (JRC-ZRO-1), TiO_2 (JRC-TIO-4), and MgO (JRC-MGO-4) were supplied from Catalysis Society of Japan. SnO_2 (Koujundo Chemical Lab.), Nb_2O_5 (CBMM), CaO (Kishida Chemical), La_2O_3 (Kishida Chemical), NiO (Kishida Chemical), SiO_2 (Fuji Silysia Q-15) were purchased. ZnO and Co_3O_4 were obtained by calcination of their hydroxides. Al_2O_3 was obtained by calcination of γ-AlOOH (Catapal B Alumina purchased from Sasol). All the metal oxide supports were calcined at 500 °C for 3 h.

2.2. Catalyst characterizations

Transmission electron microscopy (TEM) images of $Ag + CeO_2$ catalyst were taken by a JEOL JEM-2010 electron microscope working at a voltage of 200 kV. High resolution TEM observation of $Ag + SnO_2$ was performed on a Hitachi High-Tech H-9500 with accelerating voltage of 300 kV. ESR spectra were measured by an X-band JEOL JES-TE200 spectrometer at a microwave power level (1.0 mW) at which saturation of the signals did not occur. The magnetic field was calibrated with a JEOL NMR field meter ES-FC5. Prior to the ESR measurements, the samples were exposed to a flow of a gas mixture of $1\%H_2$/He at 573 K for 30 min, cooled to room temperature under a flow of pure He, exposed to a flow of a gas mixture of $10\%O_2$/He at room temperature for 5 min, and purged with He at room temperature for 5 min. Then, ESR spectra were measured at −196 °C. X-ray diffraction (XRD) patterns were recorded on a Rigaku diffractometer MiniFlex-II operated at 30 kV and 15 mA using Ni-filtered Cu-Kα radiation. Patterns were collected using a step size of 0.02° and a scan speed of 1° min^{-1} in the range of 20° to 80°.

Ag K-edge XAFS measurements were performed in transmission mode at the BL01B1 in the SPring-8 (Proposal No. 2007A1224, 2008A1633). The storage ring was operated at 8 GeV. A Si(1 1 1) single crystal was used to obtain a monochromatic X-ray beam. Samples were sealed in cells made of polyethylene under ambient atmosphere and XAFS spectra were taken at room temperature. The analysis of the extended X-ray absorption fine structure (EXAFS) was performed using the REX version 2.5 program (RIGAKU). The Fourier transformation of the k^3-weighted EXAFS oscillation from k space to r space was performed over the range 40–140 nm^{-1} to obtain a radial distribution function. The inversely Fourier filtered data were analyzed with a usual curve fitting method in the k range of 40–140 nm^{-1}. For the curve-fitting analysis, the empirical phase shift and amplitude function for the Ag–Ag shell was extracted from the data for Ag foil.

2.3. Catalytic tests

The catalytic activity for soot oxidation was determined using commercially available carbon black powders (Mitsubishi Chemical Corporation, MA7; surface area 115 $m^2\,g^{-1}$, average particle size 24 nm) as model diesel soot. The carbon and a catalyst with a weight ratio of 1/20 (2 mg/40 mg) were ground for 5 min to obtain so-called tight-contact mixtures. The catalytic test was carried out with gravimetric thermal analysis (TG/DTA, Rigaku 8120). The soot/catalyst mixture was heated from room temperature to 600 °C at a rate of 5 °C min^{-1} in a stream of 20% O_2 balanced with He at a flow rate of 100 $cm^3\,min^{-1}$. The temperature that gives maximum intensity of the exothermic DTA peak (T_{max}) was used to compare soot oxidation activity of different catalyst. The effluent gas was analyzed by nondispersive infrared (NDIR) CO/CO_2 analyzers (Horiba VIA510).

The apparent activation energy of the soot oxidation is determined by the Ozawa method [45] using the following expression: $d\log(\beta)/d(1/T_\alpha) = 0.4567\,E/R$, where β is the heating rate used, T_α the temperature corresponding to α% carbon conversion, E is the apparent activation energy in kJ mol^{-1}. E can be estimated from the slope of the least squares straight line fit of $\log(\beta)$ versus $1/T_\alpha$ plot.

3. Results and discussion

3.1. Effects of calcination, metal powder, and metal oxide support on carbon oxidation

Profiles of CO_2 emission and DTA signal on carbon oxidation with pure CeO_2, Ag metal powder, and mixture of them are shown in Fig. 1. Pure CeO_2 and pure Ag metal powder showed insufficient activity for carbon oxidation, i.e., the maximum CO_2 emission

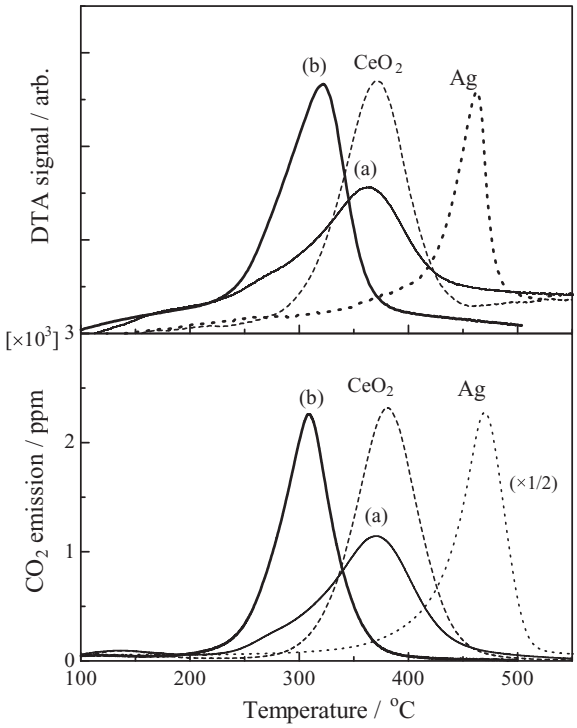

Fig. 1. DTA and CO_2 emission profiles of carbon oxidation with pure CeO_2, pure Ag metal powder, and physical mixture of Ag (20 wt%) and CeO_2 before (a) and after (b) calcination at 500 °C for 3 h in air.

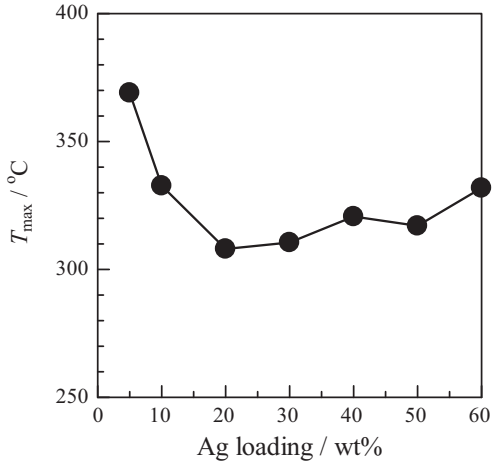

Fig. 2. Effect of Ag loading on T_{max} on carbon oxidation with Ag + CeO_2 after the calcination.

is observed at 380 °C for pure CeO_2 and at 470 °C for Ag powder, respectively. As for the physical mixture of Ag + CeO_2, the CO_2 emission profile before calcination was almost similar to that of pure CeO_2, though a part of carbon oxidation started below 300 °C. On the other hand, interestingly, a calcination of Ag + CeO_2 at 500 °C significantly decreased the temperature range of carbon oxidation and the maximum CO_2 emission was observed at 308 °C. The DTA profiles also showed similar temperature dependences to those of CO_2 emission profiles. The profile was similar to that of Ag/CeO_2 prepared by impregnation method [44]. The mechanical mixture of Ag and CeO_2 followed by calcination resulted in the formation of an active catalyst for carbon oxidation. As reported previously [44], the temperature at which the maximum extho-thermal DTA signal in carbon oxidation, T_{max}, is also used as a measure of catalytic activity in this study.

Fig. 2 shows the effect of loading amount of Ag. The minimum value of T_{max} was observed at 20 wt%. The effect of Ag loading was significant at lower Ag content, but not significant in the range of 20–30 wt%. The following investigation on the effects of metals and supports is carried out using the catalysts at 20 wt% of Ag or other metals.

Fig. 3 shows DTA profiles for carbon oxidation over physical mixtures of CeO_2 and various metal powders (Ag, Cu, Au, Pt) after calcination at 500 °C for 3 h. The physical mixtures of CeO_2 with Cu, Au, and Pt showed similar DTA profiles to that of pure CeO_2. The promotion effect of carbon oxidation was only observed when Ag powder was mixed with CeO_2.

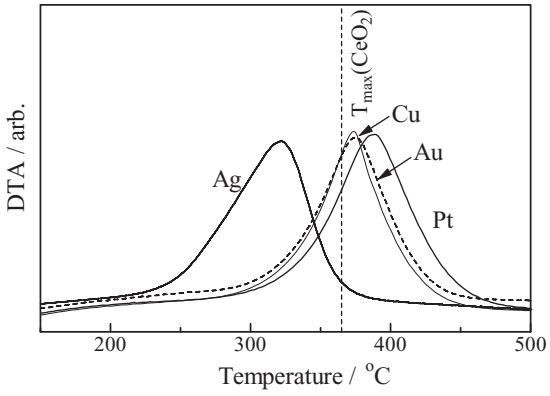

Fig. 3. DTA profiles of carbon oxidation with 20 wt% metal + CeO_2 mixture after the calcination at 500 °C for 3 h in air.

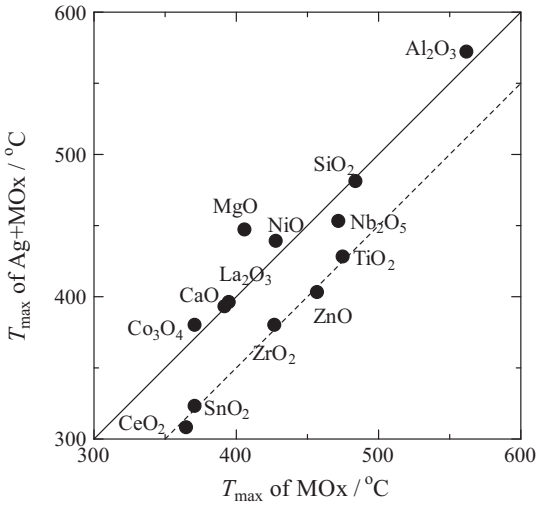

Fig. 4. Comparison of ΔT_{max} of pure metal oxides (MOx) and 20 wt% Ag + MOx mixed catalysts. The solid line shows T_{max}(Ag + MOx) = T_{max}(MOx), and the broken line shows T_{max}(Ag + MOx) = T_{max}(MOx) – 50 °C.

The effects of metal oxides as supports for Ag are also examined. In Fig. 4, the values of T_{max} of pure metal oxides (MO*x*) and T_{max} of Ag + MO*x* after calcination at 500 °C for 3 h are compared. The plots were almost on the solid line when Co_3O_4, CaO, La_2O_3, NiO, SiO_2, and Al_2O_3 were used as supports, indicating there is no effect of mixing with Ag. The plot of MgO was upper side of the solid line, indicating a negative effect of mixing with Ag. On the other hand, the supports of CeO_2, SnO_2, ZrO_2, ZnO, TiO_2, Nb_2O_5 significantly lowered the temperature of carbon oxidation. The difference in the oxidation temperature for CeO_2, SnO_2, ZrO_2, ZnO and TiO_2 was around 50 °C, and that was 15 °C for Nb_2O_5. These metal oxides are generally known as oxygen nonstoichiometry at higher temperatures. Typically, CeO_2 is known to be an oxygen-storage material due to redox between Ce^{4+} and Ce^{3+} under an oxidizing or reducing atmosphere [46–53]. SnO_2, ZnO and TiO_2 are typical n-type semiconductors depending on the formation of oxygen vacancy. The figure suggests that the formation of oxygen vacancy is a key factor for the promotion effect of carbon oxidation. The role of oxygen vacancy will be discussed in Section 3.3.

3.2. Characterization of Ag species

Ag + CeO_2 catalysts were characterized in order to clarify the unique effect. Fig. 5 shows XRD patterns of the series of Ag + CeO_2 with various Ag loading after calcination. Only the diffraction lines of CeO_2 and Ag metal were observed in the diagrams. Other diffraction lines, such as Ag_2O, were not detected. The state of Ag on Ag + CeO_2 was also investigated by Ag K-edge EXAFS (Figure not shown). The spectrum of Ag(20) + CeO_2 after calcination only showed Ag–Ag shell, of which R = 2.89 Å and coordination number = 7.6, while Ag–O shell was not clear. Comparing with the theoretical values of Ag foil (R = 2.89 Å, coordination number = 12), the smaller coordination number indicates high dispersion of Ag metal particles on CeO_2. The results of XRD and Ag K-edge EXAFS clarified that the phase of Ag on CeO_2 is basically metallic state and Ag particles are finely dispersed on CeO_2 surface.

The dispersion of Ag was confirmed by TEM images. Fig. 6 shows the TEM images of Ag(20) + CeO_2 after the mechanical mixing and the calcination. Before the calcination (Fig. 6a), very wide range of distribution of Ag particles can be seen. As shown in Fig. 7a, the diameters of several Ag particles are more than 100 nm, while most of the particles are below 100 nm. The average diameter of Ag was 66 ± 46 nm before calcination. On the other hand, only small

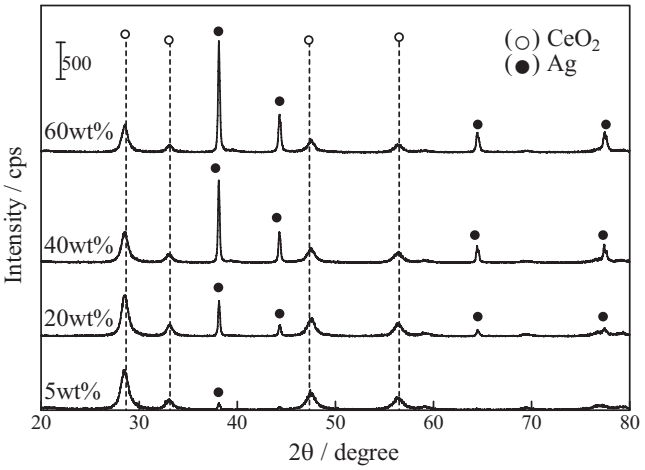

Fig. 5. XRD patterns of Ag + CeO_2 after mixing followed by the calcination.

particles less than 10 nm can be seen in Ag(20) + CeO_2 after the calcination (Fig. 6b), while large Ag particles are not. The particle size of Ag became smaller with very narrow distribution (7.6 ± 1.4 nm), as shown in Fig. 7b. It was clarified that Ag particles were self-dispersed drastically during the calcination.

The drastic self-dispersion of Ag was also observed on Ag + SnO_2, as shown in the TEM image in Fig. 8. The large particles having the diameter with more than 10 nm can be assigned to tetragonal SnO_2, which was supported by XRD patterns. On the other hand, the presence of Ag particles was not clear. At least, the TEM image indicates that Ag is not in the large particle but well-dispersed in the small particles.

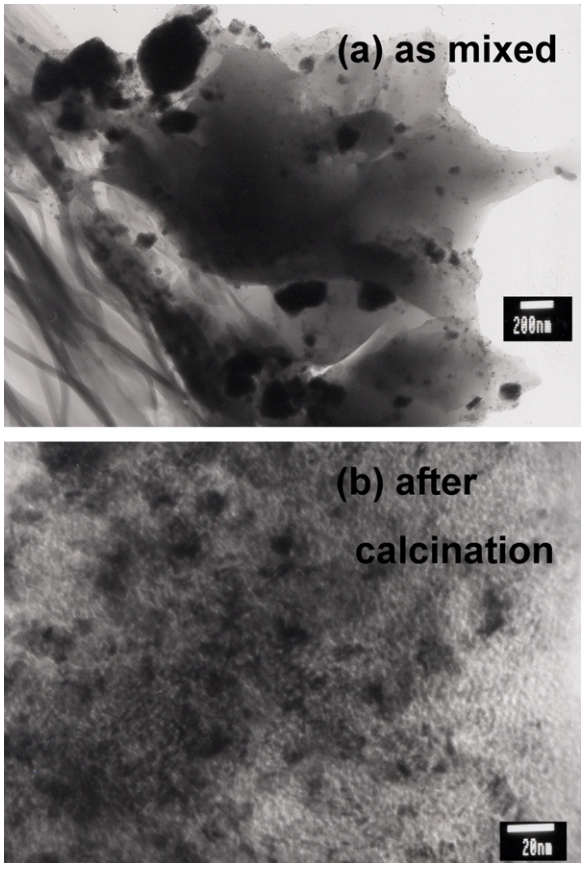

Fig. 6. TEM images of Ag(20) + CeO_2 (a) after mixing, and (b) after the calcination.

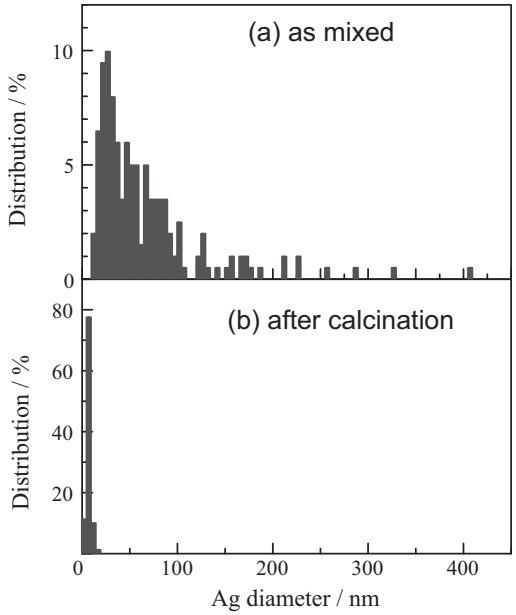

Fig. 7. Size distribution of Ag particles in Ag(20) + CeO_2 (a) after mixing, and (b) after the calcination observed in TEM images.

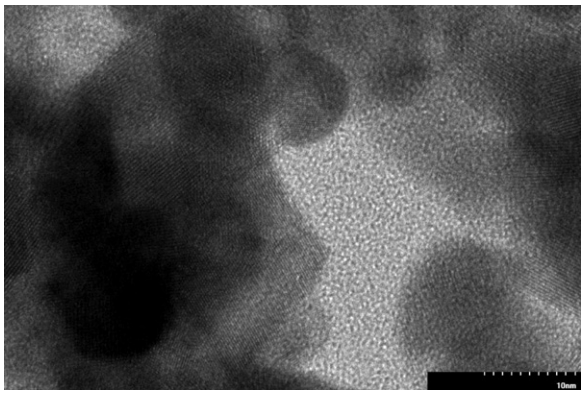

Fig. 8. TEM image of Ag(20) + SnO_2 after mixing followed by the calcination.

The apparent activation energy of carbon oxidation by Ag(20) + CeO_2 was evaluated by Ozawa plot, and compared with those of CeO_2 and Ag_2O in Table 1. Since the carbon/catalyst ratio is 1/20 in the present study, the activation energies of CeO_2 and Ag_2O are somewhat different from those reported in the previous paper, which were measured with the carbon/catalyst ratio of 1/80 [44]. The activation energy of Ag(20) + CeO_2 was far lower than that of pure CeO_2 but close to that of Ag_2O. The similar trend was also observed for Ag/CeO_2 prepared by impregnation method [44]. The results indicates that Ag_2O-like species is the active species on Ag(20) + CeO_2. However, XRD and EXAFS data demonstrated that the bulk phase of dispersed Ag is Ag metal. Furthermore, only a part of carbon was oxidized over Ag(20) + CeO_2 in a flow of He without

Table 1
Apparent activation energies for carbon oxidation under 20% O_2/N_2 (E_{O_2}) or under pure He (E_{He}) with pure CeO_2, pure Ag_2O, Ag(20) + CeO_2 prepared by mixing and calcination.

Catalyst	E_{O_2}/kJ mol^{-1}	E_{He}/kJ mol^{-1}
CeO_2	127	144
Ag_2O	81	81
Ag(20) + CeO_2	91	94

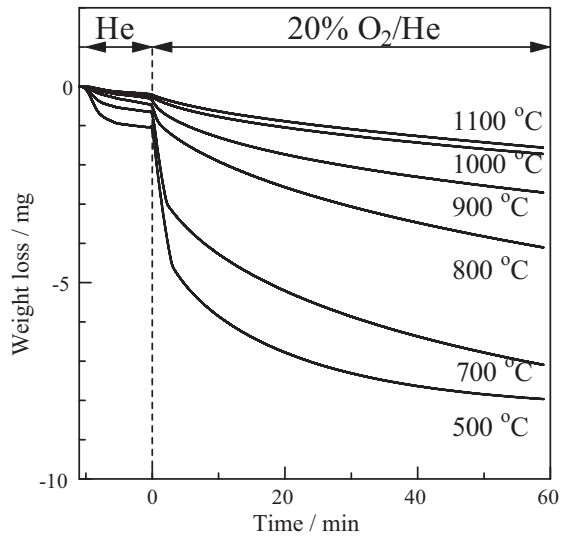

Fig. 9. Effect of calcination temperature of CeO_2 on carbon oxidation at 350 °C with Ag(20) + CeO_2 after the calcination.

O_2, while Ag_2O showed similar CO_2 emission profiles in the presence and absence of O_2. Therefore, only limited part of external surface layer and/or interface between CeO_2 and Ag particles should be oxidized and act as Ag_2O-like species for carbon oxidation. In Aneggi's report, the carbon oxidation activity of Ag/CeO_2 was lower than those of Ag/ZrO_2 and Ag/Al_2O_3, and the lower activity was attributed to too much stabilized interface of Ag/CeO_2 connected by Ag_2O intermediate layer [37]. In our study, such intermediate phase was not detected. It can be speculated that the higher catalytic activity of Ag + CeO_2 than Ag + ZrO_2 in our study may be due to the absence or negligible amount of stable Ag_2O-intermediate layer between Ag particle and CeO_2 surface. The formation of unstable Ag_2O-like species on the external surface of Ag nano-particles and/or interface of Ag and CeO_2 should act as the active species for carbon oxidation.

3.3. Controlling factor for self-dispersion

CeO_2 was calcined at various temperatures from 500 to 1100 °C, mixed with 20 wt% of Ag power, calcined at 500 °C for 3 h in air, and the catalytic activities for carbon oxidation with the obtained Ag + CeO_2 were compared at 350 °C. Fig. 9 shows the weight loss during carbon oxidation with Ag + CeO_2. The carbon/catalyst mixture was heated in a flow of He up to 350 °C, and carbon oxidation was started by switching the flow gas to 20% O_2/He. It is clear that the weight of carbon/catalyst mixture steeply decreased when CeO_2 was calcined below 700 °C, while the decay curves were gradual when CeO_2 was calcined above 800 °C. From the transient response of weight loss, the initial rate and the rate constant k were determined by assuming the first order reaction, and the values are shown in Table 2. Both the initial rates and the rate constants decreased with the calcination temperature of CeO_2 and a gap was observed between 700 and 800 °C. One may expect that the decrease in the rate constant is due to the sintering of CeO_2. However, the contribution of sintering of CeO_2 to the activity gap is not high, because significant decrease in the surface area was observed in the different region between 800 and 900 °C. The results in the table suggest that the catalytic activity is controlled by another factor.

In Section 3.1, a contribution of oxygen vacancy of the supports to the promotion effect of carbon oxidation was suggested. Since the contribution of self-dispersion of Ag during the calcination was suggested to be a factor of promotion of carbon oxidation

Table 2
Effect of calcination temperature on surface area and ESR signals of CeO_2, and rate of carbon oxidation at 350 °C with Ag(20) + CeO_2.

Calcination temperature/°C	Surface area/$m^2\ g^{-1}$	Initial rate/10^{-6} mol s^{-1}	Rate constant k/$10^{-3}\ s^{-1}$	ESR signal[a]/arb.
500	119	1.80	4.0	69.2
700	48	1.30	3.5	57.3
800	15	0.23	1.1	6.7
900	5.9	0.32	1.1	3.7
1000	2.7	0.14	0.9	3.6
1100	1.8	0.10	0.7	1.4

[a] Normalized by surface area.

with Ag + CeO_2 and Ag + SnO_2 (Section 3.2), the oxygen vacancy may contribute to the self-dispersion of Ag. In order to evaluate the concentration of oxygen vacancy, the oxygen vacancy is estimated by the activated oxygen detected by ESR.

Fig. 10 shows ESR spectra recorded at −196 °C for CeO_2 calcined at various temperatures. The CeO_2 samples were at first reduced in 1%H_2/He at 300 °C for 30 min, cooled to room temperature under a flow of pure He, exposed to a flow of 10% O_2/He for 5 min at room temperature, and purged with He at room temperature before the measurement. After the adsorption of O_2, a strong signal with anisotropic g parameters of g_{xx} = 2.009, and g_{zz} = 2.035 was observed. The signal can be assigned to O_2^- superoxide ion formed by the following equation [35,54,55].

$$Ce^{3+}\text{–}V_O + O_2 \rightarrow Ce^{4+}\text{–}(O\text{–}O)^- \qquad (V_O\text{: oxygen vacancy})$$

The intensity of the signal strongly depends on the calcination temperature of CeO_2, i.e., it was strong below 700 °C, while significantly diminished above 800 °C. The integrated intensities of the ESR sig-

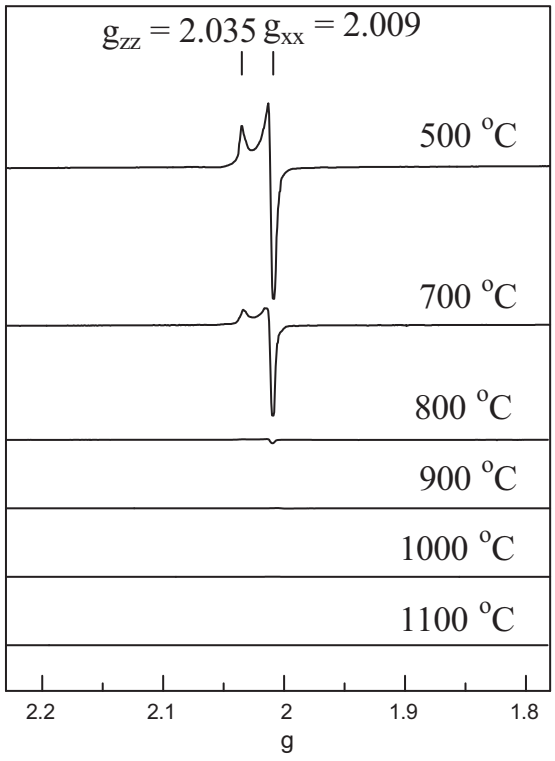

Fig. 10. ESR spectra recorded at −196 °C K for CeO_2 calcined at various temperatures for 3 h. Before the measurements, CeO_2 samples were reduced in 1%H_2/He at 300 °C for 30 min, cooled to room temperature in a flow of He, exposed to a flow of 10% O_2/He for 5 min, and purged with He at room temperature before the measurement.

nals are listed in Table 2. The dependences of the activity for carbon oxidation and the ESR signal on calcination temperature of CeO_2 are in a good agreement. The gaps were observed between 700 and 800 °C in both the cases. The results indicate that the formation of oxygen vacancy of CeO_2 should be the important factor for the self-dispersion of Ag into nano-particles.

It can be speculated that there are two major factors for the self-dispersion of Ag particles under the oxidative atmosphere. One is oxidation of Ag as a driving force of dispersion and the second is strong interaction between Ag and CeO_2. The former was also observed during H_2-assisted HC-SCR over Ag/Al_2O_3 and Ag/MFI [56–60]. By using in situ UV–vis and EXAFS, it was revealed that Ag particles were easily oxidized into Ag^+ ions under oxidative atmospheres. Supported Ag was reversibly transformed to Ag^+ ions under oxidative atmospheres and to $Ag_n^{\delta+}$ clusters under reductive atmospheres. Villani et al. also reported the reversible change of Ag species on Al_2O_3 between oxidized and reduced atmospheres [20]. The heating of Ag/Al_2O_3 in the presence of NO*x* resulted in the formation of $AgNO_3$, which showed high catalytic activity for carbon oxidation with decomposition into finely dispersed metallic Ag and Ag_2O. The catalyst can be regenerated in cycles involving cooling and heating in the presence of NO*x*. The activity dependence on oxygen vacancy of CeO_2 (Table 2) suggests a contribution of oxygen vacancy to dispersion of Ag^+ ions. The adsorption of gaseous O_2 on the vacant site results in the formation of active oxygen species, which can oxidize outer Ag atom of Ag metal particles into Ag^+ ions. The formed Ag^+ ions spill over on the surface of CeO_2 and disperse. As shown in Table 1, the lowering the oxidation temperature was obtained on the metal oxides having oxygen nonstoichiometry, which supports the role of oxygen vacancy on self-dispersion of Ag.

As for the interaction between Ag and the supports, highly dispersed Ag species have strong interaction with anionic sites of the support such as ion-exchange sites of zeolites [57–59]. Actually, the size of $Ag_n^{\delta+}$ clusters depends on the strength of acid sites. In the case of CeO_2 surface, anionic sites on surface oxygen act as an acceptor of Ag^+ ion. The stabilization of Ag on CeO_2 can be related to well-known phenomenon of re-dispersion of Pt on CeO_2 as reported by Nagai et al. [61]. In their case, Pt^{2+} or Pt^{4+} ions are fixed on CeO_2 by forming Pt-O-Ce bond under an oxidative atmosphere at 800 °C, and a low temperature reduction results in the formation of small Pt metal particles. In the case of $Ag + CeO_2$, the reduction process is not required because Ag_2O thermally decomposes into Ag metal above 200 °C [62], which is lower than the calcination temperature at 500 °C. Therefore, it can be proposed that the self-dispersion of Ag under the calcination in air at 500 °C proceeds with the following steps: (1) oxidation of large Ag particles and formation of Ag^+ ions or small silver oxide clusters, (2) these species are easily dispersed on metal oxide supports by electrostatic interaction with CeO_2 surface, (3) several Ag ions partially agglomerates, (4) at the same time silver oxides are thermally decomposed into Ag metal nano-particles.

4. Conclusion

A novel strategy for preparation of Ag/CeO_2 catalysts for carbon oxidation is demonstrated. Calcination of a physical mixture of $Ag + CeO_2$ at 500 °C in air results in self-dispersion of Ag into nano-particles and significant enhancement of catalytic activity for carbon oxidation. The bulk phase of Ag nano-particle is Ag metal. Since the activation energy of $Ag + CeO_2$ was comparable to that of Ag_2O, partially oxidized parts of Ag particles, probably external surface or interface between CeO_2, act as active species for carbon oxidation. Oxygen vacancy of CeO_2 is suggested to be an important factor for the self-dispersion of Ag into nano-particles.

Acknowledgements

This work was partly supported by a Grant-in-Aid for Scientific Research B (20360361) from the Japan Society for the Promotion Science. The X-ray absorption experiment was performed with the approval of the Japan Synchrotron Radiation Research Institute (Proposal No. 2007A1224).

References

[1] B.A.A.L. van Setten, M. Makkee, J.A. Moulijn, Catal Rev. 43 (2001) 489.
[2] J.P.A. Neeft, M. Makkee, J.A. Moulijn, Appl. Catal., B 8 (1996) 57.
[3] J.P.A. Neeft, F. Hoornaert, M. Makkee, J.A. Moulijn, Thermochim. Acta 287 (1996) 261.
[4] W.F. Shangguan, Y. Teraoka, S. Kagawa, Appl. Catal. B: Environ. 8 (1996) 217.
[5] Y. Teraoka, S. Kagawa, Catal. Surv. Jpn. 2 (1998) 155.
[6] Y. Teraoka, K. Nakano, S. Kagawa, Appl. Catal., B 34 (2001) 73.
[7] S.S. Hong, G.D. Lee, Catal. Today 63 (2000) 397.
[8] D. Fino, P. Fino, G. Saracco, V. Specchia, Appl. Catal. B: Environ. 43 (2003) 243.
[9] D. Uner, M.K. Demirkol, B. Dernaika, Appl. Catal. B: Environ. 61 (2005) 334.
[10] J. Liu, Z. Zhao, C. Xu, A. Duan, T. Meng, X. Bao, Catal. Today 119 (2007) 267.
[11] J. Liu, Z. Zhao, C.-M. Xu, A.-J. Duan, Appl. Catal. B: Environ. 78 (2008) 61.
[12] D. Reichert, H. Bockhorn, S. Kureti, Appl. Catal. B: Environ. 80 (2008) 248.
[13] C. Badini, G. Saracco, V. Serra, V. Specchia, Appl. Catal. B: Environ. 18 (1998) 137.
[14] M. Ogura, K. Morozumi, S.P. Elangovan, H. Tanada, H. Ando, T. Okubo, Appl. Catal. B: Environ. 77 (2008) 294.
[15] H. An, C. Su, P.J. McGinn, Catal. Commun. 10 (2009) 509.
[16] J. Oi-Uchisawa, A. Obuchi, S. Wang, T. Nanba, A. Ohi, Appl. Catal. B: Environ. 43 (2003) 117.
[17] J.O. Uchisawa, S. Wang, T. Nanba, A. Ohi, A. Obuchi, Appl. Catal. B: Environ. 44 (2003) 207.
[18] G. Corro, J.L.G. Fierro, F.B. Romero, Catal. Commun. 7 (2006) 867.
[19] K. Villani, C.E.A. Kirschhock, D. Liang, G. Van Tendeloo, J.A. Martens, Angew. Chem. Int. Ed. 45 (2006) 3106.
[20] K. Villania, R. Brosiusa, J.A. Martens, J. Catal. 236 (2005) 172.
[21] E.E. Miró, F. Ravelli, M.A. Ulla, L.M. Cornaglia, C.A. Querini, Catal. Today 53 (1999) 631–638.
[22] M.L. Pisarello, V. Milt, M.A. Peralta, C.A. Querini, E.E. Miró, Catal. Today 75 (2002) 465–470.
[23] B. Dernaika, D.A. Uner, Appl. Catal. B: Environ. 40 (2003) 219.
[24] M.N. Bokova, C. Decarne, E. Abi-Aad, A.N. Pryakhin, V.V. Lunin, A. Aboukaïs, Thermochim. Acta 428 (2005) 165.
[25] M.A. Peralta, V.G. Milt, L.M. Cornaglia, C.A. Querini, J. Catal. 242 (2006) 118.
[26] A. Bueno-López, K. Krishna, M. Makkee, J.A. Moulijn, Catal. Lett. 99 (2005) 203.
[27] A. Bueno-López, K. Krishna, M. Makkee, J.A. Moulijn, J. Catal. 230 (2005) 237.
[28] K. Krishna, A. Bueno-López, M. Makkee, J.A. Moulijn, Appl. Catal. B: Environ. 75 (2007) 189.
[29] K. Krishna, A. Bueno-López, M. Makkee, J.A. Moulijn, Appl. Catal. B: Environ. 75 (2007) 201.
[30] K. Krishna, A. Bueno-López, M. Makkee, J.A. Moulijn, Appl. Catal. B: Environ. 75 (2007) 210.
[31] A. Bueno-López, K. Krishna, B. van der Linden, G. Mul, J.A. Moulijn, M. Makkee, Catal. Today 121 (2007) 237.
[32] X. Wu, D. Liu, K. Li, J. Li, D. Weng, Catal. Commun. 8 (2007) 1274.
[33] T. Masui, K. Minami, K. Koyabu, N. Imanaka, Catal. Today 117 (2006) 187.
[34] K. Ito, K. Kishikawa, A. Watajima, K. Ikeue, M. Machida, Catal. Commun. 8 (2007) 2176–2180.
[35] M. Machida, Y. Murata, K. Kishikawa, D. Zhang, K. Ikeue, Chem. Mater. 20 (2008) 4489.
[36] E. Aneggi, C. de Leitenburg, G. Dolcetti, A. Trovarelli, Catal. Today 114 (2006) 40–47.
[37] E. Aneggi, J. Llorca, C. de Leitenburg, G. Dolcetti, A. Trovarelli, Appl. Catal. B: Environ. 91 (2009) 489.
[38] Q. Liang, X. Wu, X. Wu, D. Weng, Catal. Lett. 119 (2007) 265.
[39] M. Dhakad, T. Mitshuhashi, S. Rayalu, P. Doggali, S. Bakardjiva, J. Subrt, D. Fino, H. Haneda, N. Labhsetwar, Catal. Today 132 (2008) 188.
[40] S.B. Simonsen, S. Dahl, E. Johnson, S. Helveg, J. Catal. 255 (2008) 1.
[41] I. Atribak, A. Bueno-López, A. García-García, J. Catal. 259 (2008) 123.
[42] T. Ishihara, T. Oishi, S. Hamamoto, Catal. Commun. 10 (2009) 1722.
[43] G. Zhang, Z. Zhao, J. Liu, G. Jiang, A. Duan, J. Zheng, S. Chen, R. Zhou, Chem. Commun. 46 (2010) 457.
[44] K. Shimizu, H. Kawachi, A. Satsuma, Appl. Catal. B: Environ. 96 (2010) 169.
[45] M. Ozawa, M. Kimura, A. Isogai, J. Alloys Compd. 193 (1993) 73.
[46] H.C. Yao, Y.F. Yu Yao, J. Catal. 86 (1984) 254.
[47] T. Miki, T. Ogawa, M. Haneda, N. Kakuta, A. Ueno, S. Tateishi, S. Matsuura, M. Sato, J. Phys. Chem. 94 (1990) 6464.
[48] T. Bunluesin, H. Cordatos, R.J. Gorte, J. Catal. 157 (1995) 222.
[49] C. Binet, A. Badri, J.-C. Lavalley, J. Phys. Chem. 98 (1994) 6392.

[50] Y. Sakamoto, K. Kizaki, T. Motohiro, Y. Yokota, H. Sobukawa, M. Uenishi, H. Tanaka, M. Sugiura, J. Catal. 211 (2002) 157.
[51] J.A. Rodriguez, J.C. Hanson, J.Y. Kim, G. Liu, A. Iglesias-Juez, M. FernLndez-GarcMa, J. Phys. Chem. B 107 (2003) 3535.
[52] J. el Fallah, S. Boujana, H. Dexpert, A. Kiennemann, J. Majerus, O. Touret, F. Villain, F. Le Normand, J. Phys. Chem. 98 (1994) 5522.
[53] T. Yamamoto, A. Suzuki, Y. Nagai, T. Tanabe, F. Dong, Y. Inada, M. Nomura, M. Tada, Y. Iwasawa, Angew. Chem. Int. Ed. 46 (2007) 9253.
[54] C. Li, K. Domen, K. Maruya, T. Onishi, J. Am. Ceram. Soc. 111 (1989) 7683.
[55] V.V. Pushkarev, V.I. Kovalchuk, J.L. d'Itri, J. Phys. Chem. B 108 (2004) 5341.
[56] A. Satsuma, J. Shibata, A. Wada, Y. Shinozaki, T. Hattori, Stud. Surf. Sci. Catal. 145 (2003) 235.
[57] J. Shibata, K. Shimizu, Y. Takada, A. Shichi, H. Yoshida, S. Satokawa, A. Satsuma, T. Hattori, J. Catal. 227 (2004) 367.
[58] J. Shibata, Y. Takada, A. Shichi, S. Satokawa, A. Satsuma, T. Hattori, Appl. Catal. B: Environ. 54 (2004) 137.
[59] A. Satsuma, J. Shibata, K. Shimizu, T. Hattori, Catal. Surv. Asia 9 (2005) 75–85.
[60] K. Shimizu, M. Tsuzuki, K. Kato, S. Yokota, K. Okumura, A. Satsuma, J. Phys. Chem. C 111 (2007) 950.
[61] Y. Nagai, T. Hirabayashi, K. Dohmae, N. Takagi, T. Minami, H. Shinjoh, S. Matsumoto, J. Catal. 242 (2006) 103.
[62] D.R. Line (Ed.), CRC Handbook of Chemistry and Physics on CD-ROM, Version 2009, CRC Press, Taylor & Francis Group, 2009.